The Design of Slushflow Barriers: CFD Simulations

Rebecca Anne Jones

Faculty of Industrial Eng., Mechanical Eng., and Computer Science
University of Iceland
2019

THE DESIGN OF SLUSHFLOW BARRIERS:

CFD Simulations

Rebecca Anne Jones

30 ECTS thesis submitted in partial fulfillment of a
Magister Scientiarum degree in Mechanical Engineering

Advisors
Halldór Pálsson
Ásdís Helgadóttir

Examiner
Vigfús Arnar Jósefsson

Faculty of Industrial Eng., Mechanical Eng., and Computer Science
School of Engineering and Natural Sciences
University of Iceland
Reykjavík, October 2019

The Design of Slushflow Barriers:
CFD Simulations
The Design of Slushflow Barriers
30 thesis submitted in partial fulfillment of a Magister Scientiarum degree in Mechanical Engineering

Faculty of Industrial Eng., Mechanical Eng., and Computer Science
School of Engineering and Natural Sciences
University of Iceland
Reykjavik
101, Reykjavik

Telephone: 525 4000

Bibliographic information:
Rebecca Anne Jones, 2019, The Design of Slushflow Barriers:CFD Simulations, M.Sc. degree, Faculty of Industrial Eng., Mechanical Eng., and Computer Science, University of Iceland.

Printing:Háskólaprent, Fálkagata 2, 107 Reykjavík
Reykjavik, October 2019

Abstract

Due to the cost of human lives near avalanche and slushflow prone locations, it is important to understand these flows and their interaction with dam barrier protection in a laboratory set-up. A previous project constructed a small-scale inclined chute that observed different dam configurations (Ágústsdóttir 2019).

In this thesis, the experiment's observations were used to verify results of 2-D CFD (Computerized Fluid Dynamics) calculations, since those are known to have a possible risk of inaccuracy and delusive results. The software, OpenFOAM, was used to construct a mesh, establish boundary conditions, and calculate flow characteristics to replicate the experiment's high-Reynolds behavior and measurements.

Comparison of experimental and simulated velocity, flow thickness, splash and hydraulic jump heights to find the most accurate match with the experiment. The simulation's cell size, 0.05 m by 0.025 m, and roughness height of 0.002 m produced the most similar profile with the experiment. For further observations, dams were constructed individually with arrangements similar to the experiment. Parameter results showed that a 95° simulated dam was most similar to the experiment, and a 34° dam was least similar. With the exception of initial splash differences, the case with two small dams was also similar with the experiment.

This thesis was able to show that 2-D CFD simulations can accurately predict velocity and Froude number parameters, but poorly predict splash and hydraulic jump heights. The simulations can be used to the benefit of fast and low-cost elements at least for velocity and Froude number predictions.

Útdráttur

Vegna manntjóns nærri áhættusvæða snjóflóða og krapaflóða er mikilvægt að skilja hegðun þeirra og hvernig snjóflóðaveggir hafa áhrif á flæði þeirra. Í fyrra verkefni var smíðuð smækkuð hallandi renna sem kannaði mismunandi hannanir snjóflóðavarna (Ágústsdóttir 2019).

Í þessu verkefni voru þær tilraunaniðurstöður nýttar til þess að staðfesta niðurstöður úr tvívíðum tölulegum hermunum, því vitað er að slík líkön geta verið ónákvæm og óáreiðanleg. Forritið OpenFOAM, var notað til þess að smíða reikninet, skilgreina jaðarskilyrði og reikna eiginleika flæðisins til þess að framkalla flæði með háa Reynoldstölu líkt og í tilraununum.

Samanburður á hraða, flæðisþykkt, hæð hæstu skvetta og straumstökkshæðar líkans og tilrauna var notaður til þess að fá sem bestu samsvörun milli líkans við tilrauna. Stærð sella 0.05 m x 0.025 m og hrýfi 0.002 m gaf bestu samsvörun. Þá voru skoðaðir varnargarðar með sömu uppsetningu og í tilraununum.

Samanburður líkans og tilrauna sýndu að 95° stífla gaf líkustu niðurstöður og 34° stífla ólíkustu niðurstöður. Að undanskilinni hæstu hæð skettu var tilfellið með tveimur litlum stíflum einnig líkt í tilraunum og líkani.

Þetta verkefni sýndi að tvívíð töluleg nálgun getur á nákvæman hátt spáð fyrir um hraða og Froude tölu flæðis en á erfitt með að spá fyrir um hæð hæstu skvetta og hæð straumstökks. Slíkt líkan má því nýta til að finna hraðan og Froude tölu krapaflóða á fljótlegan og ódýran máta.

Contents

List of Figures ix

List of Tables xi

Variable Names xiii

Acknowledgements xv

1 Introduction 1

2 Theory 3
2.1 Navier-Stokes Equations . . . 3
2.2 Reynolds Averaged Navier-Stokes modeling . . . 3
2.3 Characteristics of Free Surface Flow . . . 4

3 Methods 7
3.1 OpenFoam . . . 7
3.2 Mesh Generation . . . 7
3.2.1 Block and Mesh Construction . . . 7
3.2.2 Boundary Conditions . . . 9
3.3 Post Processing of CFD . . . 11
3.3.1 Phase Fraction . . . 11
3.3.2 Velocity . . . 11
3.3.3 Roughness . . . 12
3.3.4 Froude number reference . . . 12
3.3.5 Splash Height . . . 12
3.3.6 Hydraulic Jump . . . 13
3.3.7 Volume . . . 13

4 Results and Discussion 15
4.1 Flow Without Barriers . . . 15
4.2 Impermeable Dam . . . 18
4.2.1 Without Breaking Mounds . . . 18

4.2.2 With Breaking Mounds 29

5 Conclusion **33**

Bibliography **35**

List of Figures

3.1 Example drawing used as a guide for building the block mesh in the simulation (Ágústsdóttir 2019). 8

3.2 An example of the final mesh construction where the green line represents the catching dam. The magnified view of the mesh at the dam's location shows the mesh sizes incrementally condensing at locations closer to the dam and the bottom wall. 9

3.3 Boundary type names where dams are also designated as walls. The figure shows the measured distances in mm. The blue wall represents the dam configuration with one small dam and the orange walls represent the two small dams configuration. The probe's location is provided to visualize the location of the measured velocity and water phase. 11

3.4 Example of splash height measurement in `ParaView`. 12

3.5 Example of hydraulic jump height measurement in `ParaView`. . . . 13

4.1 The experiment's Froude number was used as reference to find the best roughness for the simulation (Ágústsdóttir 2019). The baseline thickness was calculated from the Froude number equation. The red line represents the experiment's calculated value, and the blue dots represent the four different roughness values calculated in the simulation. 16

4.2 Velocity results with a volume of 2.7 m^3 and without barriers. The red, blue, and yellow lines are from experiment measurements (Ágústsdóttir 2019). The purple line is the measured velocity from the simulation. 17

4.3 Initial splash height main catching dam positioned at 34°. 18

4.4 Initial splash height main catching dam positioned at 60°. 19

4.5 Initial splash height main catching dam positioned at 75°. 20

4.6 Initial splash height main catching dam positioned at 90°. 21

4.7 Initial splash height main catching dam positioned at 95°. 22

4.8 Initial splash height main catching dam positioned at 100°. 23

4.9 Hydraulic jump height main catching dam positioned at 34°. 24

4.10 Hydraulic jump height main catching dam positioned at 60°. 25

4.11 Hydraulic jump height main catching dam positioned at 75°. 25

4.12 Hydraulic jump height main catching dam positioned at 90°. 26

4.13 Hydraulic jump height main catching dam positioned at 95°. 26

4.14 Hydraulic jump height main catching dam positioned at 100°. . . . 27

4.15 Initial splash height of one small dam. 29

4.16 Initial splash height of two small dams. 30

List of Tables

4.1 List of various cell sizes in the x (direction of flow) and y-direction (direction of structure's depth) with parameters observed in simulations. The "x" column represents the size of the cell in the x-direction, and "y" column represents the size of the cell in the y-direction. These cell sizes are located closest to the Main Catching Dam and the bottom of the channel. The thickness measured from ParaView and the average velocity measured at 2.5 seconds. 15

4.2 Comparison between Experiment (Ágústsdóttir 2019) and Simulation water flow results for the Main Catching Dam configuration. . 28

4.3 Small dam measurements from the experiment (Ágústsdóttir 2019) and the simulation. 31

Variable Nomenclature

ϵ	Dissipation Rate
Fr	Froude number
$\mathbf{g}$	Gravity
h	Depth of Flow (Height Before Hydraulic Jump)
k	Turbulent Kinetic Energy
K	Mean Kinetic Energy
p	Pressure
ρ	Density
S_M	Momentum due to Source Rate of Increase
τ	Stress
t	Time
u	Flow speed
$\mathbf{v}$	Velocity Vector
ν_t	Turbulent Viscosity
μ	Viscosity
$y+$	Distance from a wall
y_1	Height Before Hydraulic Jump
y_2	Height After Hydraulic Jump

Acknowledgements

To Katrín Helga Ágústsdóttir for conducting experiment measurements, providing data, and ensuring a smooth transition from the experiment. I would like to thank Viðar Guðmundsson and the Physics Department of the University of Iceland for providing computing resources and encouragement to push outside of known capabilities.

I would like to thank my supervisors Ásdís Helgadóttir and Halldór Pálsson of the University of Iceland. Their productive feedback, encouragements, and patience has contributed to my growth, development, and academic accomplishments at this university.

1 Introduction

Slushflow hazard is an ongoing issue throughout various regions of the world (Jaedicke 2016). It is a destructive phenomenon that is not only financially expensive, but is more importantly a hazard to human life (Hestnes 1996).

Slushflow is the flow of dense water-saturated snow (Gauer 2004), which results from snowpack combined with water accumulation, water level rise, and rapid thawing (Hestnes 1996). When snowpack weight and gravity exceeds friction of the basal path, a turbulent flow is released depending on the properties of the path (Hestnes 1996). This flow behavior also depends on the impermeable ground, steepness, terrain composition, and water composition (Hestnes 1996). Ultimately, slushflows may cause large waves in fjords and lakes (Hestnes 1996).

Hazard control is one of the mainframes for slushflow mitigation, which is the focus in this thesis (Hestnes and Sandersen 2000). One of the several measures mentioned in a previous work, "Main principles of slushflow hazard mitigation' (Hestnes and Sandersen 2000), is catching dams and walls. This type of control work is applied when the velocity and the size of slushflows is known (Hestnes and Sandersen 2000). The dams are positioned in a channel that diverges the flow to a favorable area away from populated areas (Hestnes and Sandersen 2000). The construction of such dams can be of concrete or steel (Hestnes and Sandersen 2000).

Slushflow experiments and CFD simulations were conducted for similar chute varieties. Techniques used in a previous experiment involved measuring velocity, pressure, flow height, and stresses with sensors (Petursson et al. 2019). These techniques were similar to the previous project which constructed the small-scale inclined chute (Ágústsdóttir 2019). The measurements were focused on pressure plates that imitated walls or barriers where normal, shear, and drag forces were found (Petursson et al. 2019).

Another different experiment used a 3-D simulation which observed flow depth, velocity, and pressure impulses (Jaedicke et al. 2008). In this case, they mixed

water with snow for slush experiments (Jaedicke et al. 2008). The model involved multiphase, non-newtonian, "Volume of Fluid" method to modify the inlet speed and depth of the flow (Jaedicke et al. 2008). The experiment not only measured the flow with velocity sensors, but was also calculated using the drag factor from the pressure measurements (Jaedicke et al. 2008). This thesis does not include pressure measurements.

Various different barriers were recently tested at a laboratory in Iceland to find the best design for flood mitigation (Hakonardottir 2019). Experiments were conducted in a small-scale flooding channel constructed in the Icelandic Road and Coastal Administration facilities to replicate slushflow scenarios where several different configurations of dams were tested (Hakonardottir 2019). Water was used to represent the flood scenario where the flow characteristics were observed and measured (Hakonardottir 2019).

The purpose of this thesis is to investigate the accuracy of OpenFoam Computational Fluid Dynamics (CFD) modeling by comparing simulation results with experiment measurements conducted in the laboratory. The accuracy of the model can be determined with the comparison of several parameters, such as flow thickness and speed. If determined suitable, further studies can be conducted at the advantage of low-cost computations rather than building expensive experimental demonstrations.

2 Theory

2.1 Navier-Stokes Equations

Newtonian fluid is described by Navier-Stokes equations, which is collective of momentum (Newton's Second Law) and continuity (mass conservation) equations. Keeping in mind the velocity vector for the x-component is

$$\mathbf{v} = \left(\mathrm{u}\mathbf{i}, \mathrm{v}\mathbf{j}, \mathrm{w}\mathbf{k}\right) \tag{2.1}$$

where u, v, and w are the velocities components in the x, y, and z directions. The continuity equation for an incompressible flow particle is

$$0 = \frac{\partial u}{\partial x} + \frac{\partial v}{\partial y} + \frac{\partial w}{\partial z} \tag{2.2}$$

In vector form, the conservation of mass equation is

$$\nabla \cdot \mathbf{u} = 0 \tag{2.3}$$

Newton's Second Law produces the Navier-Stokes equation in vector form, represented as

$$\rho \frac{D\mathbf{v}}{Dt} = \rho\mathbf{g} - \nabla p + \mu\nabla^2\mathbf{v} \tag{2.4}$$

where ρ is density, μ is the viscosity, p is the pressure, $\mathbf{g}$ is the gravity vector. $\frac{D\mathbf{v}}{Dt}$ is the material derivative, defined as $\frac{\partial v}{\partial t} + \mathbf{u} \cdot \nabla$ where time is represented by t. The energy equation is not included due to the assumption that heat transfer is insignificant in these experiments.

2.2 Reynolds Averaged Navier-Stokes modeling

Turbulent flows characterized with a high Reynold's number and random velocity fluctuations requires complex computations. Velocity, $u = \bar{u} + u'$, and pressure,

$p = \bar{p} + p'$, follow the fluctuating rules. The fluctuating properties incorporated into the Navier-Stokes equation (x-component) is

$$\frac{\partial \bar{u_i}}{\partial t} + \bar{u_j}\frac{\partial \bar{u_i}}{\partial x_j} = -\frac{1}{\rho}\frac{\partial \bar{p}}{\partial x_i} + \frac{1}{\rho}\frac{\partial}{\partial x_j}\left(\mu\frac{\partial \bar{u_i}}{\partial x_j} - \rho\bar{u_i'u_j'}\right) \tag{2.5}$$

The k-ϵ model is a type of two-equation turbulence model used for the purpose of CFD calculations. In this model, the k represents turbulent kinetic energy and ϵ represents the dissipation rate. Turbulent kinetic energy is expressed as

$$k = \frac{1}{2}\left(\bar{u^2} + \bar{v^2} + \bar{w^2}\right) \tag{2.6}$$

where the transport equation for turbulent kinetic energy is

$$\frac{\partial k}{\partial t} + u_j\frac{\partial k}{\partial x_j} = \frac{\partial}{\partial x_j}\left(\frac{\nu_t}{\sigma_k}\frac{\partial k}{\partial x_j}\right) + \nu_t\left(\frac{\partial u_i}{\partial x_j} + \frac{\partial u_j}{\partial x_i}\right)\frac{\partial u_i}{\partial x_j} - \epsilon \tag{2.7}$$

The turbulent viscosity is defined as

$$\nu_t = \rho C_\nu \frac{k^2}{\epsilon} \tag{2.8}$$

where $C_\nu = 0.09$ and $\sigma_k = 1.0$. The dissipation rate, ϵ, is expressed as

$$\epsilon = 2v\bar{e_{ij}'e_{ij}'} \tag{2.9}$$

where e_{ij}' is the fluctuating rate of deformation. The transport equation for turbulent dissipation ϵ is

$$\frac{\partial \epsilon}{\partial t} + u_j\frac{\partial \epsilon}{\partial x_j} = \frac{\partial}{\partial x_j}\left(\frac{\nu_t}{\sigma_\epsilon}\frac{\partial \epsilon}{\partial x_j}\right) + C_1\frac{\epsilon}{k}\nu_t\left(\frac{\partial u_i}{\partial x_j} + \frac{\partial u_j}{\partial x_i}\right)\frac{\partial u_i}{\partial x_j} - C_2\frac{\epsilon^2}{k} \tag{2.10}$$

where $C_1 = 1.44$, $C_2 = 1.92$, and $\sigma_\epsilon = 1.3$. Turbulent viscosity applies when considering boundary conditions for the ramp and dams.

2.3 Characteristics of Free Surface Flow

The Froude number was used to compute and compare the thickness of the water stream in the laboratory experiment and the simulation. This equation is a dimensionless ratio between inertia and gravitational forces with respect to different flow regimes (Furniss et al. 2006)

$$\mathrm{Fr} = \frac{u}{\sqrt{gy_1}} \tag{2.11}$$

where u is the velocity, g is gravity, and y_1 is thickness of flow (also known as the height before the hydraulic jump). To establish the thickness of the flow after a hydraulic jump, the following equation is used (White 2008):

$$\frac{y_2}{y_1} = \frac{1}{2}\left(1 + 8\mathrm{Fr}_1^2 - 1\right) \tag{2.12}$$

where y_2 is the height after the hydraulic jump.

3 Methods

3.1 OpenFoam

The solutions were calculated with OpenFOAM version 6, which performs CFD numerical computations (OpenFOAM Foundation 2019). Meshing was constructed with the `blockMesh` application according to the domain for the channel. ParaView version 5.4 was used for post-processing visualization of CFD solutions (Ayachit 2015).

The solver, `interFoam`, was used due to the experiment providing two incompressible fluids that are isothermal and immiscible (Joao et al. 2018). The simulation used the volume-of-fluid (VOF) method, which is used for multiphase flows (Heyns and Oxtoby 2014).

The following numerical schemes were calculated during OpenFOAM simulations: the time scheme was transient, first order implicit, and bounded; and gradient scheme was Gaussian and linearly interpolated. Most divergence terms were Guassian with second order, unbounded interpolation schemes. The exceptions are that the `alpha` term (water volume) used the `vanLeer` scheme, and the convection term used a second order, upwind scheme.

3.2 Mesh Generation

3.2.1 Block and Mesh Construction

The block mesh was constructed according to the following steps:

1. Referencing the experiment's construction

- Drawings produced from the experiment were used as a reference to create coordinates for the `blockMesh` construction (Ágústsdóttir 2019).

- The dimension scale in the experiment was 1:10 (lab:field), and the same scale was assumed in the CFD computations (Ágústsdóttir 2019).

2. Simulation Model Dimensions

   - The dimensions were constructed in a 2D model.

   - The width/depth of the chute and channel were assumed to be 1 meter.

   - In the small-scale experiment, the tank was slightly narrower than the chute. The tank's length in the simulation was decreased by 0.196 m to compensate for this difference.

   - The channel in the simulation was elongated to over five meters beyond the main catching dam. This was done to better visualize the splash over the main breaking dam.

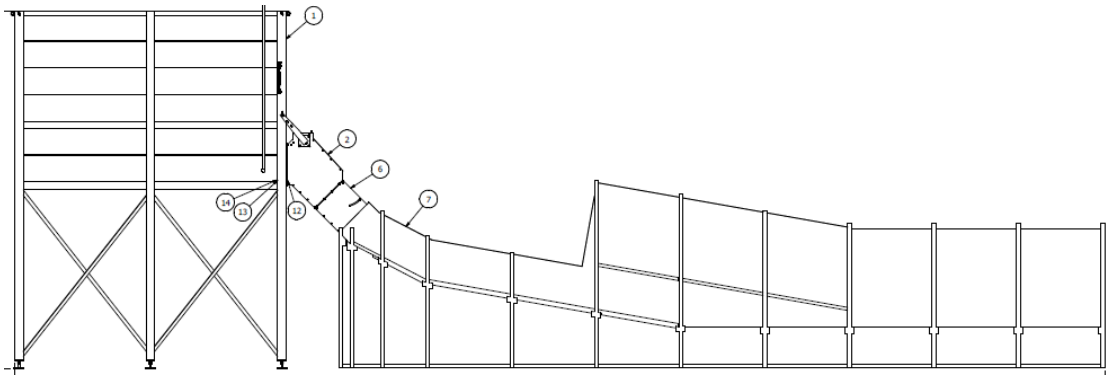

Figure 3.1: Example drawing used as a guide for building the block mesh in the simulation (Ágústsdóttir 2019).

1. Mesh Construction

   Different mesh sizes were used to find the closest results with the measured velocity from laboratory results (Ágústsdóttir 2019).

   - The initial mesh cell sizes were equal in the x and y directions.

   - Then, cell sizes were refined in the x and y directions (see Table 4.1).

- The mesh sizes closest to the bottom of the chute and the main catching dam were incrementally reduced in size with an expansion ratio. The final cell size is discussed in the results.

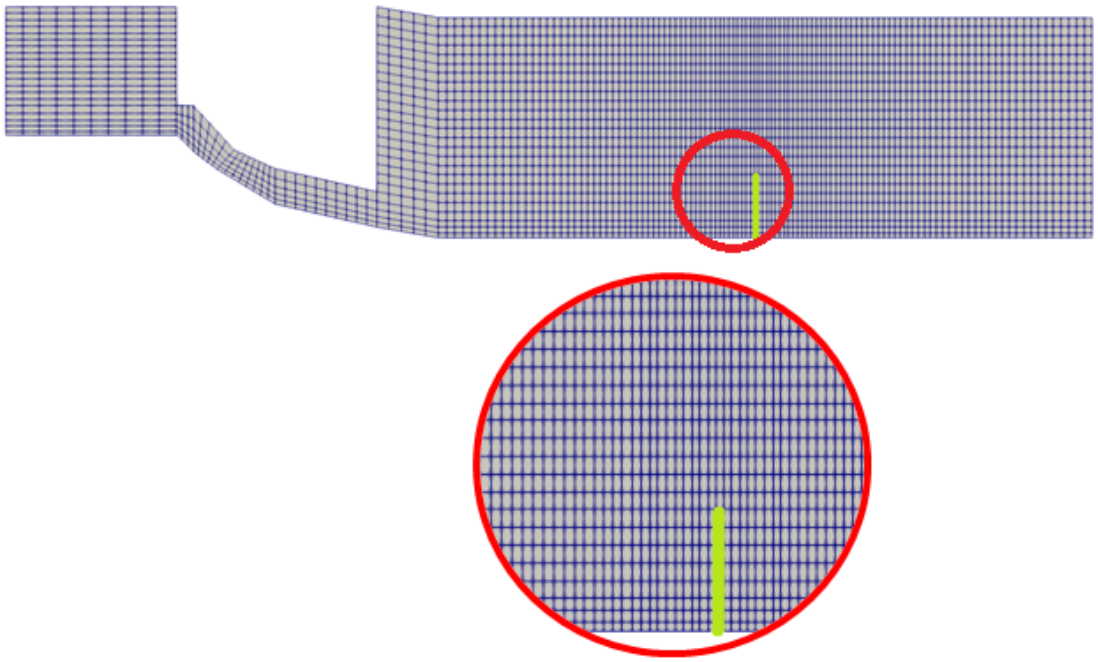

Figure 3.2: An example of the final mesh construction where the green line represents the catching dam. The magnified view of the mesh at the dam's location shows the mesh sizes incrementally condensing at locations closer to the dam and the bottom wall.

3.2.2 Boundary Conditions

The boundaries were defined in the `blockMesh` for boundary positioning, then boundary conditions were defined within the k, ϵ, ν_t, p, and u parameters.

1. Outer Walls

    - Parameters, k and ϵ, provided turbulence and dissipation wall function conditions for high-Reynolds cases.

    - The simulation used standard wall functions for high-Reynolds numbers where the distance from the wall, $y+$, is greater than what the

turbulence model requires.

- Ambient boundaries include the top of the tank, chute, and channel where the parameters, k and ϵ, have a uniform initial condition. The ν_t, p, and u parameters initially are `zeroGradient`.

- Walls located at the front and back of the entire model, tank sides and right-most edge had a "no slip" velocity condition. The initial conditions of roughness, Ks, and ϵ are uniform. The ν_t, p, and u parameters have initial values of zero.

2. Impermeable Dam Construction

   - The dams were included as wall boundaries once roughness and velocity conditions replicate the laboratory experiment behaviors.

   - Due to the varying angles of the main catching dam's position, a distorted mesh was used to change the block construction to different dam configurations.

   - The angle for every dam configuration was adjusted for every calculation.

   - Each dam configuration has a defined name and set:

     – Catching dam

     – One small dam

     – Two small dams

   - Within each set, the coordinates and size of each dam was defined.

   - Baffles were created to convert each set into vertical walls.

   - The channel was extended due to preventing the wrong type of boundary condition at the catching dam. It was also necessary to measure and view the trajectory, splash heights, and volume remaining inside the dam.

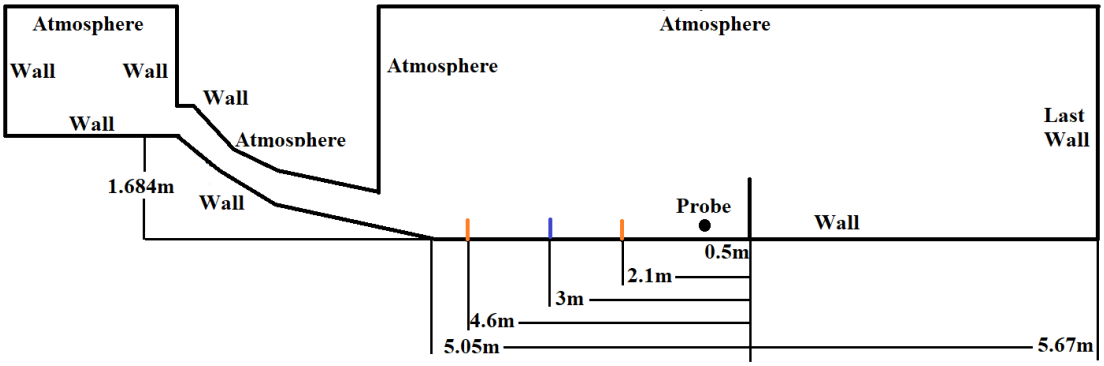

Figure 3.3: Boundary type names where dams are also designated as walls. The figure shows the measured distances in mm. *The blue wall represents the dam configuration with one small dam and the orange walls represent the two small dams configuration. The probe's location is provided to visualize the location of the measured velocity and water phase.*

3.3 Post Processing of CFD

3.3.1 Phase Fraction

The initial conditions of the water phase (`alpha.water`) are set at `zeroGradient` and range between values of 0 and 1, where 0 represents the the air phase and 1 represents the water phase. This feature was used to visualize the water flow in `ParaView` and to find the height limit of water flowing through the channel. This was useful for positioning the velocity probe in the `blockMesh`.

3.3.2 Velocity

For cases involving no dams, the velocity solution from the simulation was compared with the experiment's velocity diagrams. To replicate the experiment's velocity meter, a probe was included to measure the `alpha.water` and velocity. The simulation's probe is located 5 cm above the ramp and 50 cm from the main catching dam's position as seen in Figure 3.3. The probe's velocity measurements were recorded for comparison between the experiment and the simulation.

3.3.3 Roughness

The roughness parameter was adjusted to produce a simulated flow that is similar to the experiment. This parameter is represented with the Ks value, which is defined within the turbulent viscosity field, ν_t. A Ks value is the height of a grain of sand (OpenFOAM Foundation 2019). The Cs value is the roughness constant that is defined as 0.5 and remained constant throughout all cases. Figure 4.1 provides calculated results for each roughness size.

3.3.4 Froude number reference

In addition to the velocity parameter, the Froude number and thickness were also used to validate the roughness size. The Froude number was provided from the experiment and was used as a reference for comparison (Ágústsdóttir 2019). The thickness was measured from `ParaView` for each case. Since the simulation has a total volume of 2.7 m^3, the experiment's Froude number, 3.7, and the calculated height, 0.171 m, were used as a baseline (see Figure 4.1).

3.3.5 Splash Height

The splash height was measured in `ParaView` with the `ruler` tool, which included the height reached by the splash droplets. This method is manually measured by the user through the `ParaView` platform. Figure 3.4 shows an example measurement of splash height.

Figure 3.4: Example of splash height measurement in `ParaView`.

3.3.6 Hydraulic Jump

The hydraulic jump height was measured in `ParaView` with the `ruler` tool. The jump was measured when the water steadily flows back towards the tank without forming large breaking waves. Figure 3.5 shows an example of hydraulic height measurement method.

Figure 3.5: Example of hydraulic jump height measurement in `ParaView`.

3.3.7 Volume

The volume of water remaining inside of the channel was measured in `ParaView`. The block mesh was divided into two different sets defined as "inlet" and "exit". The division of these sets were located at the main catching dam position. Tables 4.2 and 4.3 provide `ParaView` measurements from the simulation.

4 Results and Discussion

4.1 Flow Without Barriers

Velocity and flow thickness were the primary and secondary flow characteristics compared with the experiment to find the most accurate mesh size. The experiment provided a graph (see Figure 4.2) that included measured velocities from three different trials (Ágústsdóttir 2019). The trials observed for the simulations were conducted with a water volume of 2.7 m^3 (Ágústsdóttir 2019). Based on the experiment's graph and videos, the total steady flow lasted about 5 sec (Ágústsdóttir 2019). From the experiment's graph, the velocity was around 4.8 m/ sec at time 2.5 sec (Ágústsdóttir 2019). The initial jump at time zero is not considered.

Table 4.1 shows four different simulated mesh sizes with calculated results. The mesh with x cell size 0.05 m and y cell size 0.025 m was the best fit for further simulations.

Table 4.1: List of various cell sizes in the x (direction of flow) and y-direction (direction of structure's depth) with parameters observed in simulations. The "x" column represents the size of the cell in the x-direction, and "y" column represents the size of the cell in the y-direction. These cell sizes are located closest to the Main Catching Dam and the bottom of the channel. The thickness measured from ParaView and the average velocity measured at 2.5 seconds.

x	**y**	**Flow Thickness (m)**	**Max Velocity (m/s)**	**Velocity (m/s)**
0.05	0.05	0.168	7.05	5.28
0.025	0.05	0.191	6.73	5.21
0.05	0.025	0.172	7.78	5.02
0.025	0.025	0.175	6.26	5.18

For additional confirmation, the Froude number was compared for roughness height adjustment. Figure 4.1 provides two of the three parameter results for each observed roughness height.

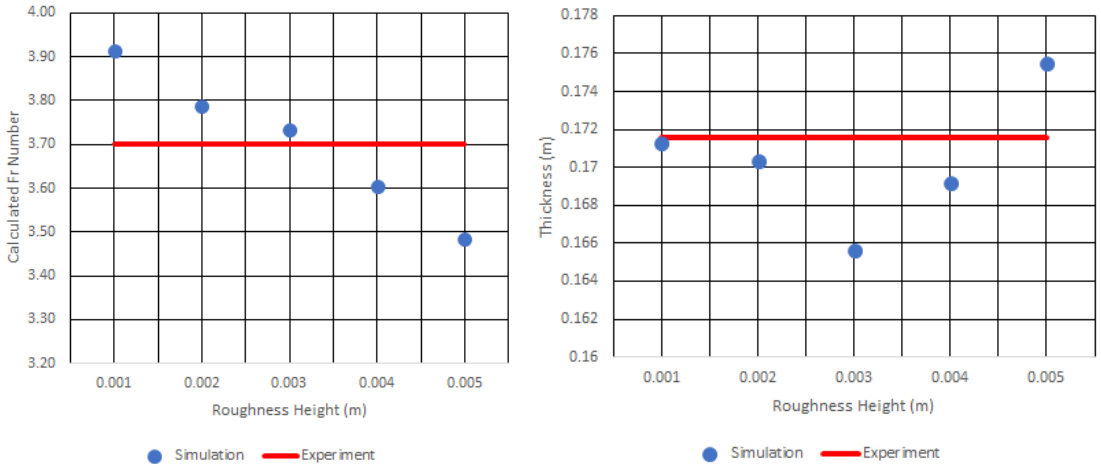

(a) Froude Number (b) Flow Thickness

Figure 4.1: The experiment's Froude number was used as reference to find the best roughness for the simulation (Ágústsdóttir 2019). The baseline thickness was calculated from the Froude number equation. The red line represents the experiment's calculated value, and the blue dots represent the four different roughness values calculated in the simulation.

The Froude number shows that the roughness height of 0.002 is the closest value to the experiment, but the flow thickness was not the closest result for this roughness. Instead, the 0.001 roughness had the closest thickness. Since thickness was measured from `ParaView's` tool, and a roughness height, 0.002, has a 0.005 m difference from the baseline thickness, this roughness height was the best match.

A visual comparison of the simulation's calculated velocity is comparable with the experiment's measured velocity in Figure 4.2. The velocity graph shows a divergence of the purple line (simulation) from the other lines (experiment) starting around 3.2 sec. The flow's reaction to the simulation's right-most barrier could be the cause of this divergence. This barrier is positioned over 5 m from where the catching dam would be located. The water impacts this barrier around 1.35 sec and begins a hydraulic jump a little over 3 sec. The water crosses back to the probe around 4 sec, and therefore flowing in the negative direction.

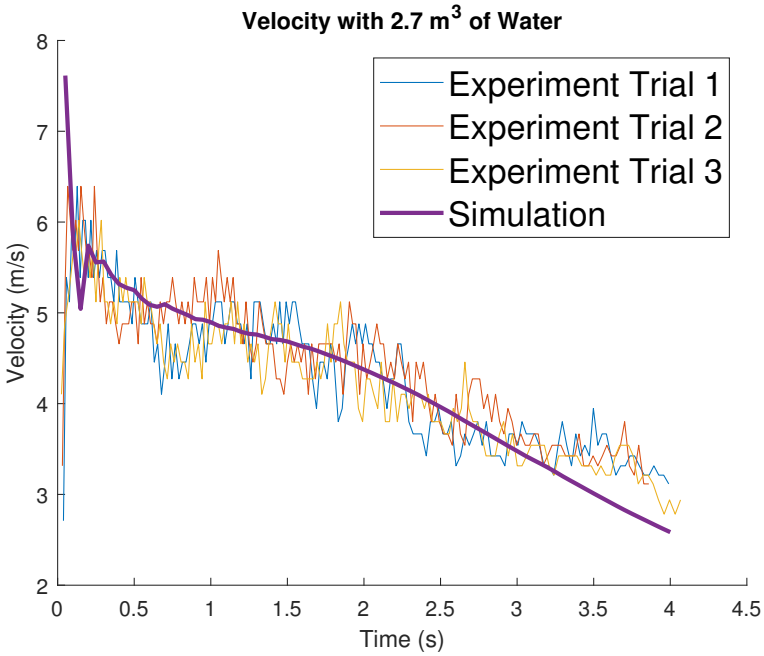

Figure 4.2: Velocity results with a volume of 2.7 m^3 *and without barriers. The red, blue, and yellow lines are from experiment measurements (Ágústsdóttir 2019). The purple line is the measured velocity from the simulation.*

The velocity graph was based on the accuracy of the experiment's measurement method and the simulation's calculation methods. Thickness and Froude's number confirm that a roughness height of 0.002m best matches the simulation.

4.2 Impermeable Dam

4.2.1 Without Breaking Mounds

Initial Splash

The water characteristics flowing through the channel with impermeable dams is provided as visual aids in Figures 4.3 to 4.8. This shows the initial splash from the experiment videos and simulations, where the simulation splash height was compared with an accuracy within ± 2 cm of the experiment. The figures are not to scale.

The flow thickness the 34° dam appears thicker and more turbulent than the simulation. The trajectory in the experiment has more droplet distribution and a different angle. The experiment's water droplets spill over the dam more vertically than the simulation. The experiment's water collecting at the top of the dam also appears thicker than the simulation.

(a) Experiment

(b) Simulation

Figure 4.3: Initial splash height main catching dam positioned at 34°.

When the experiment's dam is positioned at 60° and 75°, the flow is thicker and more turbulent than the simulations, especially at the beginning of the ramp. The simulation hooks over the dam, but the experiment sprays droplets at a similar angle of the dam. Although the 75° simulated dam collects water towards the top of the dam that is similar to the experiment, the experiment has more droplet-dispersed reaction upon impact with the dam.

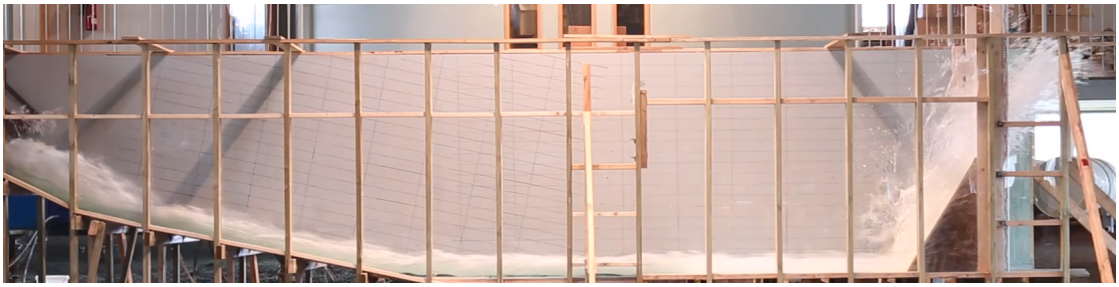

(a) Experiment

(b) Simulation

Figure 4.4: Initial splash height main catching dam positioned at 60°.

(a) Experiment

(b) Simulation

Figure 4.5: Initial splash height main catching dam positioned at 75°.

The flow also looks thicker and more turbulent along the experiment's ramp, but looks similar along the flat area when considering the dam with 90°. The experiment's flow has a reaction of more droplets upon impact with the dam where it looks like most of the water collects towards the middle of the splash and the simulation collects water towards the top of the splash. Both figures show slight narrowing of the splash at the tip.

(a) Experiment

(b) Simulation

Figure 4.6: Initial splash height main catching dam positioned at 90°.

Although the experiment's 95° dam has more turbulence and a thicker flow towards the beginning of the ramp, the experiment's flow thickness seems similar to the simulation in the flat area. The experiment's splash has a wider dispersion of droplets upon impact than the simulation. The experiment's splash appears more evenly distributed than the simulation impact where the droplets spray from the dam evenly throughout its length, but the simulation accumulates water at the top of the splash.

(a) Experiment

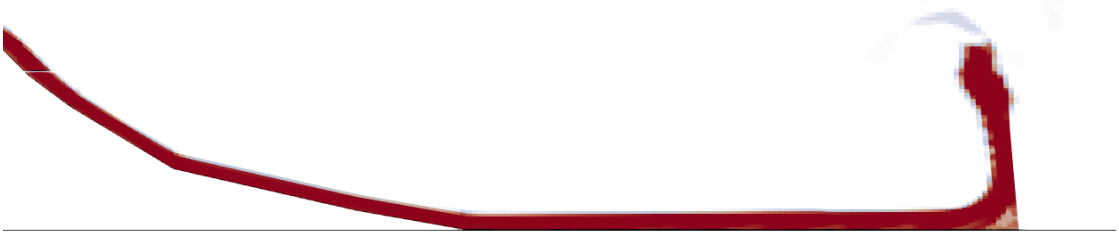

(b) Simulation

Figure 4.7: Initial splash height main catching dam positioned at 95°.

Not including the initial flow from the chute, the thickness appears similar between both 100° configuration figures. The experiment's splash reacts more drastically from impact and arches back almost uniformly along the splash's length. The simulation has less droplet distribution upon impact where the splash starts to curve back towards the top of the splash.

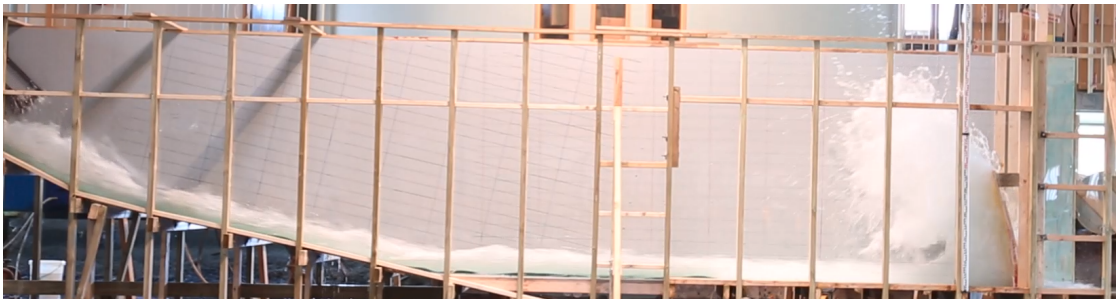

(a) Experiment

(b) Simulation

Figure 4.8: Initial splash height main catching dam positioned at 100°.

For all figures, the splash height from the simulation does not have the droplet or distribution characteristics like the experiment. This could be due to the mesh cell sizes being bigger than the droplet sizes. The material difference between the ramp and the dam used in the experiment might have a small impact on the water flow because of the different roughness values for each material.

During the initial splash, the simulations with dam angles 34° and 60° have more water distribution than the experiment. The simulations with dam angles 75°, 90°, 95°, and 100° have a bulk of water collecting at the top of the splash. The experiment shows that the water is about evenly distributed throughout the splash length. This may also be due to the simulation calculating the movement of the majority of water volume. Another reason is the possibility that the majority of water volume in the experiment is actually collecting at the top of the splash

length, but it may be difficult to see from the experiment's pictures.

Hydraulic Jump Height Comparison

Figures 4.9 through 4.14 show a visual comparison of the hydraulic jump between the experiments and the simulations. When considering the dam positioned at 34°, the simulation's hydraulic jump height is significantly thinner than the experiment. They both have enough water located on the right side of the dam. The experiment tapers at the left end of the hydraulic jump, but the simulation appears to have a consistent height throughout the jump. These simulation figures are not to scale.

(a) Experiment

(b) Simulation

Figure 4.9: Hydraulic jump height main catching dam positioned at 34°.

The dam positioned at 60° has a similar hydraulic jump height in both the experiment and the simulation. The experiment's jump is almost twice as long as the simulation and has more droplet dispersion. These similarities and differences also apply for the 75° dam. Both simulations have air pockets that are not seen in the experiment.

(a) Experiment

(b) Simulation

Figure 4.10: Hydraulic jump height main catching dam positioned at 60°.

(a) Experiment

(b) Simulation

Figure 4.11: Hydraulic jump height main catching dam positioned at 75°.

For cases of 90°, 95°, and 100° dam configurations, the hydraulic jump looks like they have similar thicknesses with the simulation with the exception of the large air pocket that forms at the top. All three cases are slightly shorter than their experiment counterpart.

(a) Experiment

(b) Simulation

Figure 4.12: Hydraulic jump height main catching dam positioned at 90°.

(a) Experiment

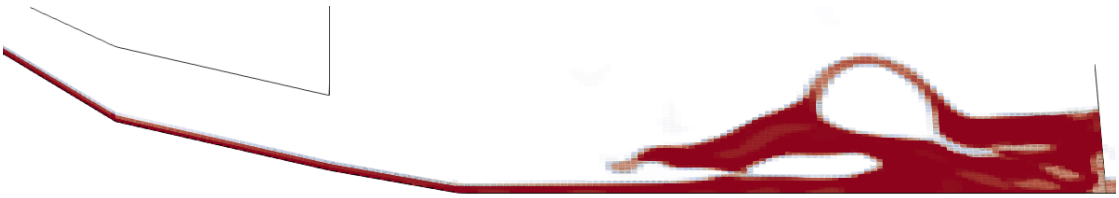

(b) Simulation

Figure 4.13: Hydraulic jump height main catching dam positioned at 95°.

(a) Experiment

(b) Simulation

Figure 4.14: Hydraulic jump height main catching dam positioned at 100°.

From these visual aids, the length of the simulated hydraulic jump is slightly shorter than the experiment. The simulation has large pockets of air in all cases, but the experiment shows a consistent composition of water throughout the hydraulic jump area. This could be caused by the 2-D model only allowing the flow to move in the x and y directions. Because the water cannot flow in the z-direction, it has to flow into the cells above or below, which may be the reason for the formation of air pockets.

Although, this can be similar to plunging breaker waves seen at the ocean shore where the high energy accumulation is broken as the wave approaches land (Buonaiuto 2018). The wave's velocity decreases as the height increases and the waves pitch forward. In this simulation, the energy accumulated from gravity is broken during impact of the dam and the flow's parameters behaved similarly.

The water flow characteristics through a channel with impermeable dams is provided in Table 4.2. This table compares the experiment and simulated results for each catching dam configuration.

Table 4.2: Comparison between Experiment (Ágústsdóttir 2019) and Simulation water flow results for the Main Catching Dam configuration.

Catching Dam								
Degrees of Catching dam			34	60	75	90	95	100
Splash Height	m	Experiment	1.30	1.80	2.20	2.10	1.90	1.70
		Simulation	1.06	1.58	2.12	1.96	1.98	1.99
Amount of Water Remaining	m^3	Experiment	2.10	2.30	2.50	2.50	2.70	2.70
		Simulation	1.16	1.89	2.13	2.46	2.50	2.54
Hydraulic Jump Height	m	Experiment	NA	0.6	0.65	0.69	0.6	0.65
		Simulation	0.27	0.62	0.68	0.61	0.65	0.72
Hydraulic Jump Time	s	Experiment	3.00	2.00	2.00	2.50	1.70	1.70
		Simulation	2.85	2.45	2.65	1.80	1.80	2.25

The splash height (including droplets) difference between the experiment and the simulation ranges from 0.04 m (75°) to 0.3 m (60°). As the dam's angle increases, the simulation's splash height measurements increase, but the experiment's splash height has a belt-curve pattern.

The volume of water remaining in the simulation's chute is less than the remaining water in the experiment. This may be due to the amount of droplets that spilled over the main catching dam in the experiments. The experiment and simulation agree that the most effective impermeable dam is the position angle of 100° and the least effective dam is 34° with regards to the volume of water remaining in the chute.

The hydraulic jump height difference between the experiment and the simulation ranges from 0.02 m (75°) to 0.13 m (90°). The timing differences ranges from 0.1 sec (95°) to 1.8 sec (34°). The experiment decreases in hydraulic jump height with the catching dam positioned at an angle of 95° and the simulation height decreases at an angle of 90°. The experiments' and the simulations' measured hydraulic jump heights are lower than the calculated hydraulic jump height (0.83 m). The hydraulic jump for position 34° was not provided.

The hydraulic timing decreases with the increase in catching dam angle, but the timing increases at 100°. The simulated dam of 95° was most similar to the

experiments and the simulated dam of 34° was least similar to the experiments.

4.2.2 With Breaking Mounds

The breaking mound initial splash heights of the simulation and the experiment is visually compared in Figures 4.15 and 4.16 where the simulation figures are not to scale. In Figure 4.15, the experiment's overall flow is more turbulent than the simulation, but the thickness along the floor looks the same. The experiment's splash trajects at a 90° angle, but the simulation trajects at a 75° angle. The height of the splash appears the same between the experiment and the simulation. There is more spray in the experiment and the simulation is more uniform.

(a) Experiment

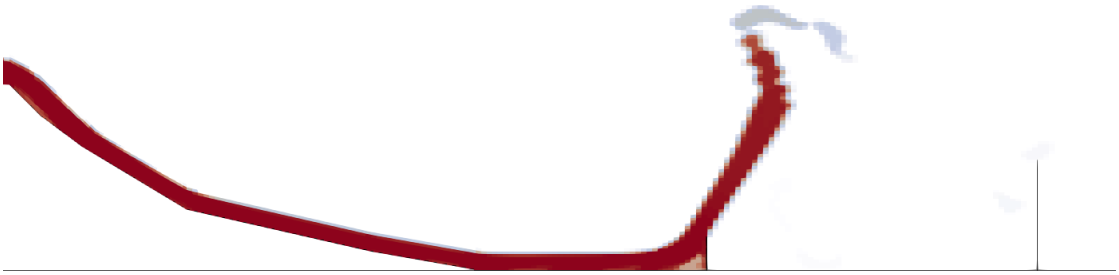

(b) Simulation

Figure 4.15: Initial splash height of one small dam.

The experiment's initial splash also has more spray or droplet dispersion than the simulation for two small dams. The experiment's splash sprays at a 90° angle with a few droplets arching back towards the beginning of the chute, but the simulation also has about a 75° trajectory from the horizon and is more uniform. Of all

simulated cases, the two small dams shows the most droplets which reach a height similar to the experiment.

(a) Experiment

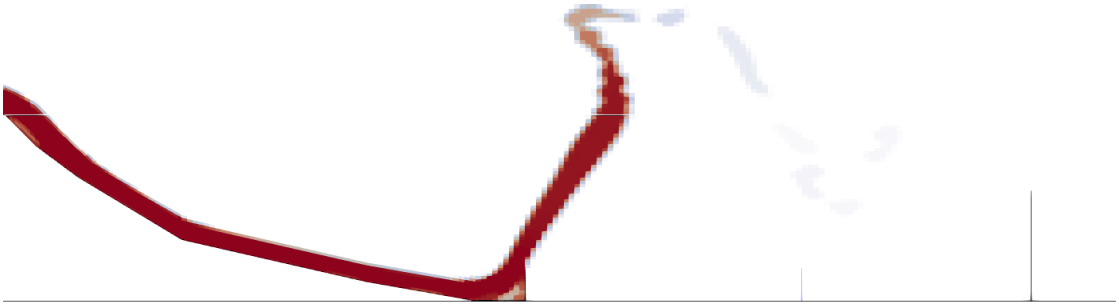

(b) Simulation

Figure 4.16: Initial splash height of two small dams.

The simulation's measured splash height for one small dam is 0.81 m and two small dams has a height that is 1.39 m higher than the experiment. The simulation's measured hydraulic jump height for one small dam is 0.14 m higher than the experiment. The hydraulic jump height for 2 small dams has little difference from the experiment.

The volume of water remaining in the chute (left of the catching dam) is very similar between the experiment and the simulations. This may be due to the contribution of the smaller dams preventing the water from splashing above the main catching dam.

Table 4.3: Small dam measurements from the experiment (Ágústsdóttir 2019) and the simulation.

			1 Small Dam	2 Small Dams
Splash Height	m	Experiment	1.60	1.30
		Simulation	2.41	2.69
Volume of Water Remaining	m^3	Experiment	2.64	2.68
		Simulation	2.66	2.69
Hydraulic Jump Height	m	Experiment	0.60	0.40
		Simulation	0.74	0.40
Hydraulic Jump Time	s	Experiment	1.80	1.25
		Simulation	3.00	1.55

When comparing between all cases, two small dams has more comparable results with the experiment. Although, this configuration does not produce the best average results among all simulated cases, the two small dams scenario case would also suffice if the initial splash height were ignored. This may be due the experiment's splash reaching above the measurement guidelines seen in Figure 4.16. Overall, it is more important to compare calculations rather than the figures due to the uncertainty of the visual characteristics.

5 Conclusion

Computational 2-D models were simulated to produce data that was compared with experimental data from small-scale laboratory experiments conducted to replicate slushflow scenarios. These tests provided flow observations and measurements for optimum barrier design.

A numerical model of a channel was developed and compared with experimental data. The modelled channel was calculated in OpenFOAM and distorted meshes were utilized to construct different dam scenarios where dam angles were changed. Without dams, the experiment's velocity and Froude number were used to construct the mesh, then the same parameters were used to program the roughness height of the channel's bottom surface. Once this was established, results for each dam configuration was calculated and produced results that were compared with the experiment measurements.

The accuracy of a CFD model was determined by finding the necessary 2-D mesh cell size, then by comparing flow parameters and characteristics with the experiment. Such observed characteristics were flow velocity, thickness, roughness, splash height, remaining volume and hydraulic jump.

When developing the 2-D block mesh, the mesh was refined into four different cell sizes. Calculations for each mesh was compared with the experiment's calculated results to find the best matching mesh. The mesh with cells sized equally in the x and y-directions produced calculations most different from the experiment. The best mesh had cells sized smaller in the y-direction than in the x-direction.

With this mesh, different roughness sizes were developed to compare the simulations' calculated parameters with the experiment's measured parameters. Results used for comparison were thickness, Froude value, and velocity. The roughness size, 0.005, was the least similar to the experiment and the roughness size, 0.002, produced the closest results.

With the best mesh and roughness sizes, the eight different dam configurations

were developed. The splash heights and hydraulic jump heights, remaining volume, and hydraulic jump timing were observed and measured with the aid of the visualization software, `ParaView`. Simulated catching dams had a different distribution of water volume during the initial splash. The 34° dam had calculated parameters least similar to the experiment and the dam with 95° had calculated parameters most similar to the experiment. With the exception of the splash height, the dam configuration with two small dams had similar calculated parameters with the experiment. For this thesis, it was best to compare the calculations from the simulation with the experiment more than comparing figures where there is visual uncertainty.

Further simulations for the the 2-D model can include pressure impulse or dam force measurements. A 3-D model can be simulated to determine if accuracy can be improved. If a 3-D model produces similar results with the 2-D model, this would help reduce computational time and power requirements.

Bibliography

Ágústsdóttir, K. (2019). *The design of slushflow barriers: Laboratory experiments*.

Ayachit, U. (2015). *The ParaView Guide: A Parallel Visualization Application*. Kitware.

Buonaiuto, F. (2018). *Waves and Water Dynamics*. Last accessed 29 June 2019. URL: http://www.geo.hunter.cuny.edu/~fbuon/GEOL_180/GEOL180_S2018_Ch8.pdf.

Furniss, M., M. Love, S. Firor, K. Moynan, A. Llanos, J. Guntle, and R. Gubernick (2006). *Froude Number and Flow States*. Last accessed 05 May 2019. URL: http://www.fsl.orst.edu/geowater/FX3/help/8_Hydraulic_Reference/Froude_Number_and_Flow_States.htm.

Gauer, P. (2004). "Numerical Modeling of a Slush Flow Event". In: *Proceedings of the International Snow Science Workshop*. Norwegian Geotechnical Institute, Oslo, Norway, pp. 19–24.

Hakonardottir, K.M. (2019). "The design of slushflow barriers: Laboratory experiments". In: Siglufjörður, Iceland, pp. 83–94.

Hestnes, E. (1996). "Slushflow hazard—where, why and when? 25 years of experience with slushflow consulting and research". In: *Annals of Glaciology* 26, pp. 370–376.

Hestnes, E. and Sandersen (2000). "The main principles of slushflow hazard mitigation". In: *Internationales Symposion Interpraevent*, p. 14.

Heyns, J. and O. Oxtoby (2014). "Modelling surface tension dominated multiphase flows using the VOF approach". In: *6th European Conference on Computational Fluid Dynamics*. Pretoria, South Africa, pp. 7082–7090.

Jaedicke, C. (2016). *RD program/ Circum - Arctic Slushflow Network (CASN)*. Last accessed 20 June 2019. URL: https://www.ngi.no/eng/Projects/Circum-Arctic-Slushflow-Network-CASN.

Jaedicke, C., MA. Kern, P. Gauer, M-A. Baillifard, and K. Platzer (2008). "Chute experiments on slushflow dynamics". In: *Cold Regions Science and Technology* 51.2-3, pp. 156–167.

Joao, M., M. Alletto, and B. Gschaider (2018). *InterFoam: OpenFoam Wiki*. Last accessed 05 May 2019. URL: https://openfoamwiki.net/index.php/InterFoam.

OpenFOAM Foundation, The (2019). *OpenFOAM v6 User Guide*. Last accessed 05 May 2019. URL: `https://cfd.direct/openfoam/user-guide`.

Petursson, H., Hafþór Örn, Hákonardóttir, Kristın Martha, and Áki. Thoroddsen (2019). "Use of OpenFOAM and RAMMS Avalanche to simulate the interaction of avalanches and slush flows with dams". In: Siglufjörður, Iceland.

White, F.M. (2008). *Fluid Mechanics, seventh edition*. New York, NY: McGraw Hill.